Gas-Phase Polymerization of Ethylene Using $MgCl_2$/Ethyl Benzoate/$TiCl_4$ + Triethylaluminum Catalyst: Effects of Triethylaluminum and Temperature

JOHN J. A. DUSSEAULT and CHENG C. HSU*

Department of Chemical Engineering, Queen's University, Kingston, Ontario, Canada K7L 3N6

SYNOPSIS

A gas-phase reactor system was developed to polymerize ethylene using the $MgCl_2$/ethyl benzoate (EB)/$TiCl_4$ + triethylaluminum (TEA) catalyst. The reproducibility of the reactor was tested and found to be adequate for kinetic study. The effects of TEA and temperature were studied with the multisite model that assumes a multiplicity of active sites. It was found that the productivity increased with Al/Ti molar ratio while initial activity leveled off. The deactivation rate, after an initial increase, decreased with Al/Ti. This corresponded with a transition in deactivation order: below Al/Ti = 70, first-order deactivation was predominant; above Al/Ti = 70, second-order deactivation was predominant. The second-order deactivation reactions were made less disperse at higher Al/Ti. Molecular weight of the polyethylene was very high (> 1,000,000) indicating negligible transfer reactions. For Al/Ti > 130 a monomer sorption limitation for polymerization was found. The effect of temperature was also studied with a maximum in productivity at 55°C for Al/Ti = 98.0 and no maximum when Al/Ti = 53.0. Apparent activation energies (E_a) for activity were found to be 19.5 ± 3.3 kJ/mol at Al/Ti = 98.0 and 9.3 ± 1.1 kJ/mol at Al/Ti = 53.0. For deactivation E_a was found to be 36.6 ± 5.0 kJ/mol at Al/Ti = 98.0 and −15.5 ± 4.4 kJ/mol at Al/Ti = 53.0. Temperature increased the dispersity of second-order deactivation reactions.

INTRODUCTION

In recent years the gas-phase polymerization process has become popular for producing polyethylene, polypropylene, and ethylene/α-olefin copolymers. The development of high-activity catalysts has made this production technology possible. However, despite the industrial popularity only a few investigations are reported in the open literature.[1,2,3] The difficulties associated with maintaining temperature control, contamination by atmospheric gases and inefficient catalyst injection, have limited research in this area. Further motivation for this work comes from the fact that research in supported Ziegler–Natta catalysts in general has concentrated on propylene polymerization, resulting in a dearth of information on ethylene polymerization.

Even in propylene polymerization our knowledge on the behavior of supported catalysts is rather limited. The complex interactions between highly reactive components, like triethylaluminum, superimposed on multiple active centers, possibly in the presence of mass transfer limitations, contribute to poor understanding.

The use of high activity catalysts, or large catalyst loadings, in slurry reactors leads to a situation where the rate of monomer consumption exceeds the rate of monomer absorption across the gas/liquid interface. When this occurs the monomer concentration does not remain at its equilibrium value. Dumas and Hsu[4] demonstrated that when this occurred for propylene polymerization the observed rate kinetics changed from acceleration-type to decay-type if the transient monomer concentration behavior was accounted for. For ethylene, the most reactive α-olefin, this situation would be exacerbated. A gas-phase reactor would avoid this potential problem.

* To whom correspondence should be addressed.

Journal of Applied Polymer Science, Vol. 50, 431–447 (1993)
 CCC 0021-8995/93/030431-17

This paper presents the gas-phase polymerization rate kinetics for ethylene using the $MgCl_2$/ethyl benzoate/$TiCl_4$ + triethylaluminum Ziegler–Natta catalyst. In particular the results of the effects of TEA and temperature will be presented and discussed.

The multisite model, originally developed by Dumas and Hsu,[5] was used with newly developed enhancements[6] to study the effects of catalyst and polymerization variables on the polymerization rate kinetics.

EXPERIMENTAL

The catalyst used in this study is the same as that used by Dumas and Hsu,[4,5] ball milling $MgCl_2$ with ethyl benzoate (EB), followed by refluxing with $TiCl_4$, and subsequent washing with *n*-heptane. Particle size was analyzed by Dumas and Hsu[4] and found that the mean aerodynamic diameter of the catalyst was $\cong$ 2 μm. The effects of catalyst and polymerization variables such as the amount of triethylaluminum, external Lewis base (ethyl benzoate), catalyst age, temperature, and monomer pressure were studied by modeling the changes in the polymerization rate kinetics. A semibatch horizontal stirred-bed reactor was used. Monomer flow rate was monitored to provide the polymerization rate as a function of time.

Materials

The compounds for the preparation of the catalyst, $MgCl_2$ (anhydrous, 98+%), ethyl benzoate (99+%), and $TiCl_4$ (99+%) were supplied by the Aldrich Chemical Company and used without further purification. Triethylaluminum (1.0 *M* in hexanes) was also obtained from the Aldrich Chemical Company.

Chemical purity ethylene (99.5%) from Matheson Gas Products was further purified by passing the gas through columns containing Drierite (H_2O absorbent), ascarite (CO_2 absorbent), alumina, and 4A, and 13X molecular sieves.

The hydrocarbon solvents (hexane and heptane) used were distilled and stored over 4A molecular sieves prior to their use.

Oxygen free nitrogen (< 5 ppm) and CO_2 were obtained from Canox Ltd. The N_2 was further purified by passing it through a Drierite column (H_2O absorbent), an OXYTRAP® (O_2 scavenger), an indicating OXYTRAP®, and 4A molecular sieves. The CO_2 was used without further purification.

Glass beads, 500-μm diameter, used as a catalyst dispersant were obtained from Spectra Abrasives Ltd.

Catalyst Synthesis

$MgCl_2$ and ethyl benzoate in a 6 : 1 molar ratio were co-milled in a 1.1 L porcelain jar, filled to $\frac{1}{4}$ to $\frac{1}{3}$ of capacity with borundum grinding cylinders, for 120 h. The resulting powder was then refluxed with an excess of $TiCl_4$ at 80°C for 2 h in a specially designed vessel. The slurry was then filtered, washed, and dried. All procedures were performed in a dry N_2 atmosphere. Complete description of the catalyst preparation can be found elsewhere.[6]

The titanium content of the catalyst was determined using the colorimetric method described by Vogel.[7] The UV-VIS absorbance was measured on a Philips 8700 spectrophotometer to give the catalyst with titanium content of 2.20 wt %.

Reactor System

A stainless steel, cylindrical horizontal stirred-bed reactor (10.2-cm diameter × 10.2-cm length) was designed and built in this work. A schematic diagram is shown in Figure 1. The catalyst, polymer, and 500-μm glass beads were mixed by three Teflon® blades attached to a shaft that rotated at 300 rpm. Two smaller and flexible Teflon® blades swept internal structures to minimize accumulations. The semibatch reactor operated at a constant monomer pressure (110–155 kPa). The rate of make-up monomer flow required to maintain the pressure, was equal to that of monomer removed from the gas-phase by polymerization, and thus was equal to the polymerization rate. This flow was measured by a Unit Instruments mass flow meter (0–1 SLM) and recorded by a Zenith Z-158 computer with a DAS-8PGA analog to digital converter. A data acquisition program, written in Turbo Basic®, recorded the data on the display screen with a real-time plot of the polymerization rate and then saved the data on floppy disk as well as creating a hard copy. The program also numerically integrated the polymerization rate curve to obtain an estimate of the yield (±7%).

Temperature control (±0.5°C) was achieved using a Yellow Springs Instruments Y-71 on/off temperature controller with a thermistor temperature probe. Flow of ethylene glycol coolant to an internal cooling coil, from a Lauda R-3 temperature bath, was regulated by a solenoid valve connected to the controller.

Water from a second bath was circulated at the reaction temperature (20–70°C) through an external

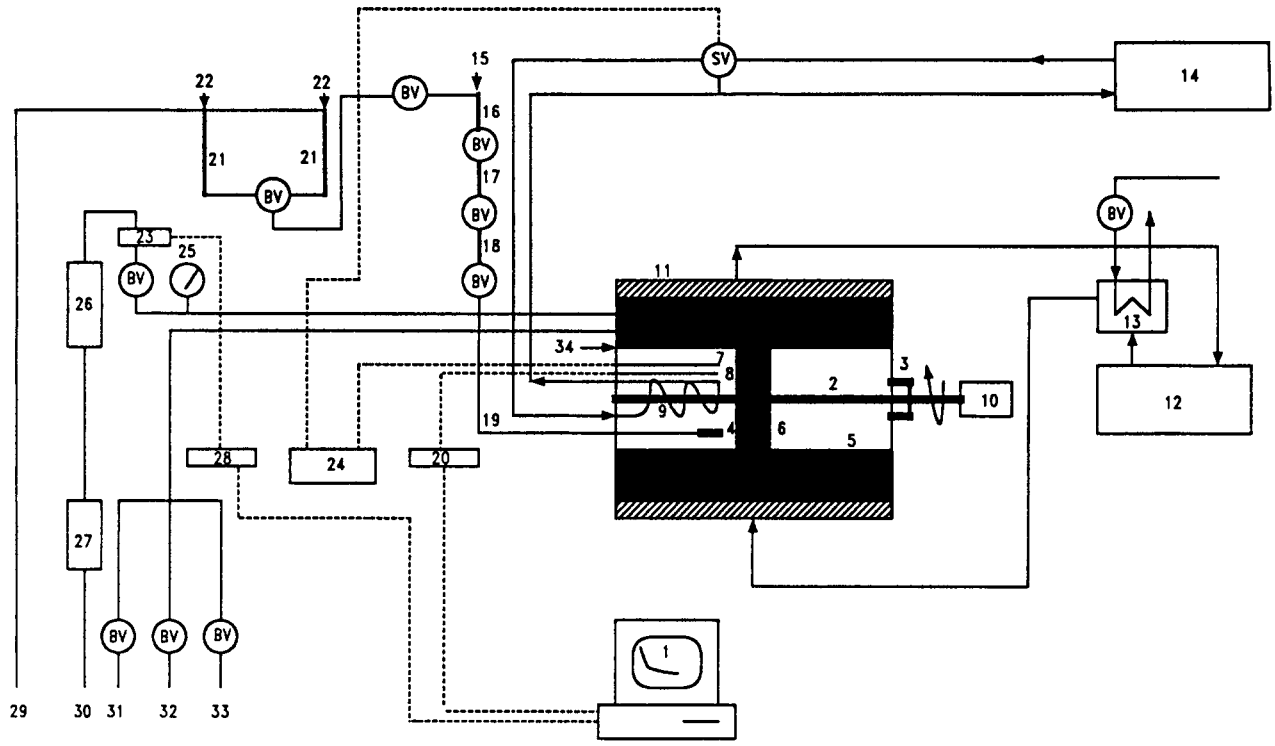

Figure 1 Schematic diagram of the reactor system. 1. Computer/data acquisition; 2. stir shaft; 3. shaft seal; 4. Teflon flow director; 5. Teflon blade; 6. blade shaft; 7. thermistor probe; 8. J-type thermocouple; 9. cooling coil; 10. drive unit; 11. external water jacket; 12. water bath; 13. heat exchanger; 14. glycol bath; 15. TEA syringe port; 16. TEA holding chamber; 17. catalyst cartridge; 18. pre-mixing chamber; 19. $\frac{1}{8}$" injection tube; 20. temperature readout; 21. hexane holding pressurization chambers; 22. syringe port; 23. mass flow meter; 24. temperature controller; 25. vacuum pressure gauge; 26. surge tank; 27. purification columns; 28. flow rate readout; 29. nitrogen source; 30. monomer source; 31. vacuum (−24 in.Hg); 32. nitrogen source; 33. high vacuum (1×10^{-1} mmHg). BV = stainless steel ball valve; SV = 3-way solenoid valve.

heat exchanger before passing through the external heating/cooling jacket of the reactor.

Temperature was measured with a J-type thermocouple and was displayed on the control board and on the computer screen. The reactor can be evacuated by the central in-house vacuum (−24 in.Hg) and by a dedicated Sargent-Welch 1400 vacuum pump (1×10^{-4} mmHg). A syringe port allows for gas samples and for CO_2 pressurization to deactivate the catalyst and terminate the polymerization.

Catalyst Addition System

The most critical aspect for a reproducible reactor system is an efficient catalyst injection system. The catalyst injection cartridge, consisting of two $\frac{1}{4}$" stainless steel Swagelok® ball valves and a 3-cm long stainless steel tube (stored under vacuum at 50°C) were transferred to the glove box. Usually 40 mg of catalyst was charged into the tube and the two valves were attached and closed. The cartridge was then connected to the premixing chamber. This assembly was then attached to the $\frac{1}{8}$" injection tube on the reactor and to the activator holding chamber. Injection was achieved by pressurizing 10 mL of hexane and washing the catalyst/cocatalyst mixture through an $\frac{1}{8}$" tube into an evacuated reactor. A second 10 mL shot of hexane was used to wash out any residual catalyst in the tubes. Mixing of the aluminum alkyl activator and catalyst powder was enhanced by the turbulent flow ($Re \cong 4 \times 10^5$) in the injection tube and by impingement on a Teflon® flow diverter at the end of the tube in the reactor. The catalyst mixture was injected upon ca. 75 g of 500-μm glass beads. This enhanced the dispersion of the catalyst throughout the reactor.

Polymerization Procedure

For a typical polymerization the reactor was brought to the reaction temperature (30–70°C) and evacuated. Catalyst was then injected into the reactor and dried for 3 min (to remove hexane solvent). The stirring was activated and polymerization begins when the reactor was pressurized with monomer (usually 110 kPa). Polymerizations usually lasted 1 h.

EXPERIMENTAL DATA REDUCTION

Monomer Concentration

There is no precise way to measure the monomer concentration at the active sites. It will be different from the bulk gas-phase concentration ($[M]_b$) because monomer will absorb into the amorphous regions of the polymer and as a consequence $[M]$ can be greater than $[M]_b$. Hutchinson and Ray[8] have closely examined this situation and concluded that Henry's law,

$$[M] = k^* P \tag{1}$$

where k^* is Henry's law constant and P the monomer pressure, is appropriate for pressures less than 40 atm. The constant, k^*, is a temperature dependent value. Hutchinson and Ray,[8] based on the work of Stern et al.,[9] suggested using the following relationship to determine k^*,

$$\log(k^*) = -2.38 + 1.08(T_c/T)^2 \tag{2}$$

where T_c is the critical temperature for the monomer (T_c = 282.4 K for ethylene). Thus at 40°C, k^* = 0.0315 mol · V_{ap}^{-1} · atm^{-1}, where V_{ap} is the volume in liters of amorphous polymer. At a reactor pressure of 110 kPa (1.086 atm) the monomer concentration would be $[M]$ = 0.0342 mol · V_{ap}^{-1}. Equations (1) and (2) can now be used to estimate $[M]$ at different pressures and temperatures.

Heat Transfer

The exothermic nature of polymerization (ΔH_p = 107.5 kJ · mol^{-1} from Floyd et al.[10,11]) makes heat transfer from the catalyst particles an important concern. If the heat dispersion is slow the particle can heat up to such an extent that the polymer formed can melt, creating problems with fusing and agglomeration. Floyd et al.[11] studied this problem using computer simulations for a gas-phase polymerization of ethylene and found that if the catalyst particle was initially small enough (diameter < 30 μm) then there were negligible intraparticle temperature gradients. The limiting factor appeared to be the transfer processes across the external film boundary layer, where again initial particle size was critical. For high-activity catalyst with a diameter of 30 μm and a particle moving at a speed of 20 cm · s^{-1}, a temperature difference across the layer was estimated at 10 K. A particle of 10 μm had a ΔT < 1 K. Floyd et al.[11] investigated differing particle velocities and found that a greater velocity lowered ΔT. The particle velocity of this reactor system, if evaluated at the edge of the stir blades, is about 163 cm · s^{-1}, eight times the largest velocity considered by Floyd et al., so ΔT in this system should be further reduced (< 1 K). There is, however, no effective way to directly measure the temperature of catalyst particles.

Finally the catalyst particle diameter for the catalysts of this study has been measured[4] as being from 0.8 to 10 μm, well below the critical values described by Floyd et al.[10,11] Thus it would appear that the build-up of significant temperature gradients within polymer particles is unlikely for this system.

Mass Transfer

Floyd et al.[10,11] have also studied the potential for monomer concentration gradients in the catalyst particle or across the external boundary layer. The boundary layer resistance was deemed insignificant, except for very large initial particles (> 60 μm) in slurry polymerization at the early stage of polymerization. In gas-phase systems this boundary layer resistance was found to be negligible.

According to Floyd et al.[10,11] the initial particle size has a profound effect on the mass transfer within the particle. If the diameter was less than 30 μm then diffusion resistance was found to be negligible for typical polymerization rates. Presence of significant diffusion resistance was identified by a change in the kinetics from decay type to an initial acceleration-type of kinetics. A monomer sorption rate limitation can also produce acceleration-type polymerization curves. If the rate at which monomer can absorb into the amorphous phase of the polymer is exceeded by the rate of monomer consumption from polymerization, then a monomer concentration gradient may exist in the particle. Criteria for the existence of this phenomenon have not been discussed in the literature. The particle size is far below 30 μm in this investigation and the diffusion in par-

ticles is expected to be negligible. The decay-type of polymerization rate curves obtained for most of the experiments conducted in this study confirmed this assertion.

Data Reproducibility

To extract meaningful information from kinetic data, the ability to reproduce data in replicate runs is of utmost importance. Figure 2 shows the plot of the specific polymerization vs. time for five runs at the same polymerization conditions. These catalyst systems are highly sensitive to any contamination, so the reproducibility exhibited here is very encouraging, especially concerning the operational procedures and the catalyst addition method. The units of specific rate in the plot and in subsequent analyses were chosen such that the rate was normalized with respect to the amount of catalyst used.

Multisite Model

Dumas and Hsu[5] originally developed a rate model that accounts for the likelihood of multiple active centers. In the original development the overall rate of polymerization for N species of active sites was given by

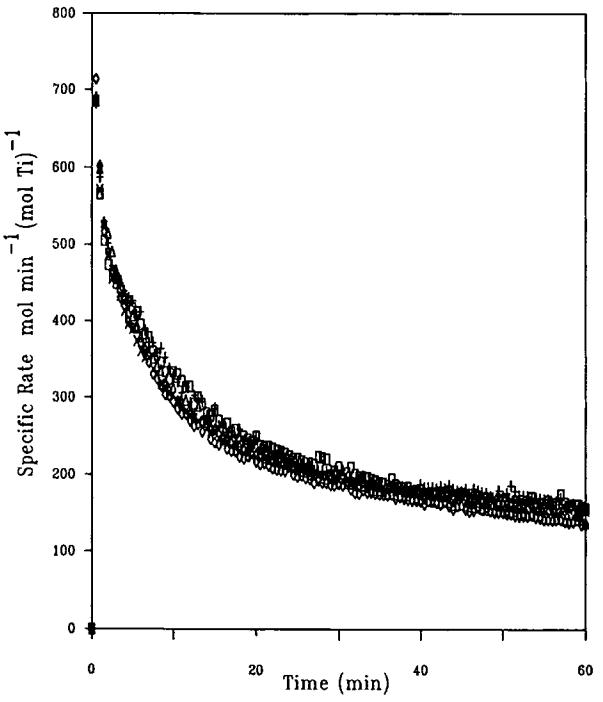

Figure 2 Reproducibility study of five polymerizations at the same polymerization conditions. Al/Ti = 87.1, 40°C, 110 kPa.

$$R_p = \sum_{i=1}^{N} k_{pi} C_i^* [M] \tag{3}$$

where k_{pi} is the propagation rate constant for species i, and C_i^* is the concentration of species i. They considered a first-order loss of sites by deactivation and developed the following rate equation

$$R_p = \frac{\theta_1 [M]}{(1 + \theta_2 \theta_3 t)^{1/\theta_3}} \tag{4}$$

with (for convenience the conditions of the summations have been neglected):

$$\theta_1 = V_T \sum k_{pi} C_{i0}^* = \sum k_{pi} N_{i0}^* \tag{5}$$

$$\theta_2 = \frac{\sum k_{pi} k_{di} C_{i0}^*}{\sum k_{pi} C_{i0}^*} \tag{6}$$

where k_{di} is the first-order deactivation rate constant and subscript 0 denotes initial condition (i.e., $t = 0$), V_T is the total volume in which the polymerization occurs and N_{i0}^* is the initial number of moles of active species i. The parameter θ_3 was described as an "empirical" dispersion parameter related to the heterogeneity of active sites.[5] However, recent work[6] has shown that when there is exclusive first-order deactivation $\hat{\theta}_3 \cong \sigma_w^2/\mu_w^2$ where $\hat{}$ signifies the least squares estimate, σ_w^2 is the weighted variance of the deactivation reactions, the weighting being the activity (k_{pi}) at each site and μ_w is the weighted mean of the deactivation rate constant (i.e., θ_2).

Other forms of polymerization rate equations are possible for different types of kinetic situations. Equation (4) is based on approximating the distribution of active sites on the catalyst with a gamma distribution. If a binomial distribution is used then the rate of polymerization is given by,

$$R_p = \theta_1 [M] \left(\frac{\beta - 1}{\beta} + \frac{1}{\beta} \exp(-\beta \nu \theta_2 t) \right)^{1/\nu} \tag{7}$$

where θ_1 and θ_2 are the same as before. β and ν can be related to the dispersity of active sites through the relation $(\beta - 1)\,\hat{\upsilon} \cong \sigma_w^2/\mu_w^2$. The choice of which model to use is determined by a deactivation profile function (DPF) plot, or rather a plot of $F(x)$ vs. x, where $x = R_p/R_{p0}$ and

$$F(x) = \frac{dR_p/dt}{dR_p/dt|_{t=0} R_p/R_{p0}}. \tag{8}$$

Figures 3 and 4 show theoretical plots for the DPFs

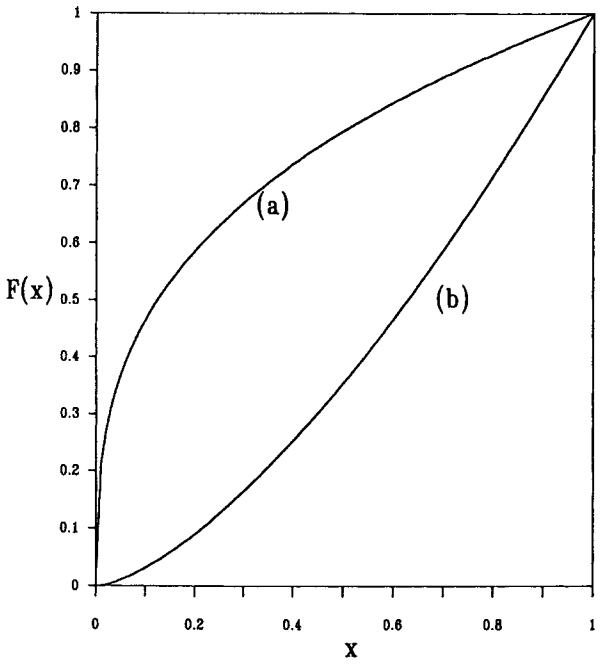

Figure 3 Theoretical deactivation profile function plot for the gamma distribution: (a) $\theta_3 = 0.333$; (b) $\theta_3 = 1.5$.

based on the gamma distribution and a binomial distribution. The behavior of a plot generated from experimental data then determines which model is appropriate. As mentioned, other model forms are possible and these are described elsewhere.[6]

It had been recognized that eq. (4), derived on the basis of first-order deactivation, can model equally well a situation where second-order deactivation prevails.[13] In such a case the meaning of θ_2 and θ_3 become unclear. Further analysis of the situation and application of recent advances in kinetic lumping theory have delineated this problem. The details of the analysis are described elsewhere.[6] The main consequence is that for second-order deactivation eq. (4) can be applied with θ_1 having the same definition, but now

$$\theta_2 = \frac{\sum k_{pi} k_{d2i} c_{i0}^{*2}}{\sum k_{pi} c_{i0}^{*}} \qquad (9)$$

or in other words the weighted average of the reciprocal of the deactivation half-life and

$$\theta_3 = 1 + (\eta + 1)/\alpha \qquad (10)$$

where $1/\alpha \cong \text{var}\,(k_p^2)/E(k_p^2)^2$ and η describes the extent of the relationship between k_{d2i}/k_{pi} and the active site ordering index i.[6] These quantities can be evaluated quantitatively only if precise information about the number of species and their constituent propagation and second-order deactivation rate constants are known. In reality these data are not available. Use of computer simulations however has shown that when $\theta_3 > 1.3$ the second-order deactivation reactions have a bimodal character classified by two groups of fast and slow deactivating sites.[6] When $1.0 < \theta_3 < 1.3$ the second-order deactivations have unimodal character. $\theta_3 = 1.0$ corresponds to a single type of second-order deactivation.

Equation (4) can obviously be applied blindly to either kinetic situation (first- or second-order) and this creates an ambiguous situation with respect to which parameter interpretation (first- or second-order) to use. This problem is solved by using the DPF plot described earlier. Computer simulation work has shown that first-order deactivation is characterized by a DPF plot with concave curvature and second-order deactivation has convex curvature.[6]

RESULTS AND DISCUSSION

Effects of Triethylaluminum (TEA)

Aluminum alkyls are highly reactive compounds and as a consequence can participate in many reactions.

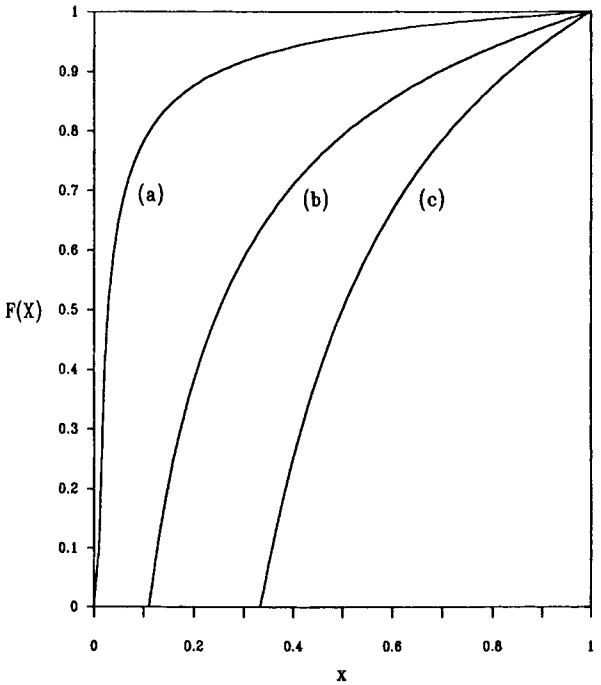

Figure 4 Theoretical deactivation profile function plot for the binomial distribution: (a) $\beta = 1.5$, $\nu = 0.5$; (b) $\beta = 1.5$, $\nu = 1.0$; (c) $\beta = 1.1$, $\nu = 0.5$.

This is true in this catalyst system where TEA reduces and alkylates $TiCl_4$; may undergo reductive metathesis reactions[14]; leaches internal EB (with which it can form a complex or react, forming aluminum alkoxide products); and reacts with impurities such as trace amounts of H_2O forming aloxanes thought to be important in some Ziegler–Natta systems.[15] It is not surprising then that the most common practice is to use TEA in stoichiometric excess of Ti, expressed in terms of a molar ratio of TEA used to the amount of catalyst used (i.e., Ti), commonly referred to as the Al/Ti ratio.

Figure 5 shows the productivity of the catalyst increasing as the Al/Ti ratio increases from 10 to 130. Unlike propylene polymerization initiated with the same catalyst, there was no maximum in productivity with respect to Al/Ti within the range studied. This could be because of the fact that both Ti^{3+} and Ti^{2+} are active for ethylene polymerization, whereas only the former is thought to be active for propylene.[16] As more TEA is used, Ti^{2+} is formed at the expense of Ti^{3+} corresponding to a loss of activity for propylene (hence a maximum), but not for ethylene. Alternatively the optimum may exist at higher value of Al/Ti than those tested; however, because of mass transfer limitations (discussed later), these values were inaccessible.

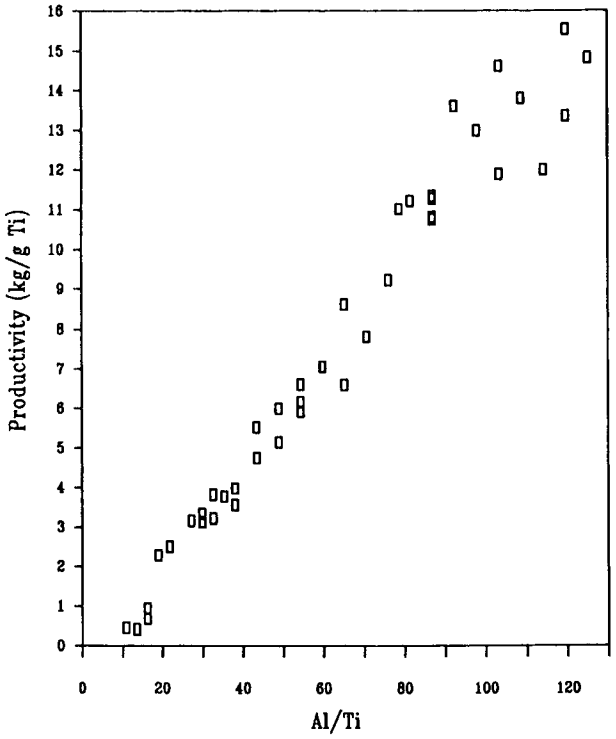

Figure 5 Productivity ($kg \cdot g^{-1}$ Ti) as a function of Al/Ti. Polymerization conditions: 40°C, 110 kPa, 1-h runs.

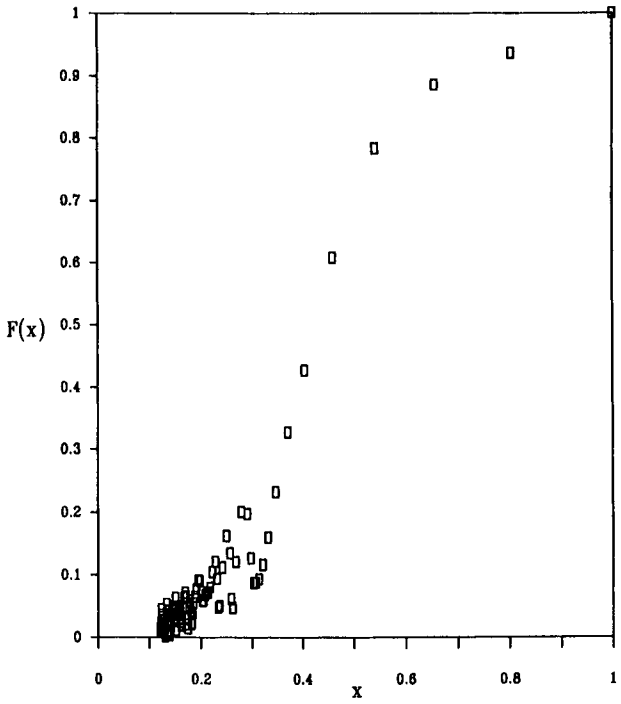

Figure 6 Deactivation profile function (DPF) plot for Al/Ti = 50. Polymerization conditions: 40°C, 110 kPa.

Previously it was discussed how the deactivation kinetics and the model form that best describes the kinetics can be identified from DPF plots. For Al/Ti ratios less than 70 the DPF typically looks like that shown in Figure 6. As x decreases from 1.0 the DPF has concave curvature, which has been shown to be evidence of first-order deactivation.[6,12] It is difficult to determine the type of curvature for the latter part of Figure 6 because of the scatter associated with this part of the DPF plot. However, a 4-h polymerization that was carried out at low Al/Ti exhibited first-order deactivation kinetics for times greater than 3 h. This result is similar to that of Keii et al.[17]

To obtain estimates of the multisite model parameters, $\hat{\underline{\theta}}$, the DPF plot suggested using eq. (7) to model the rate kinetics.

As Al/Ti approached 70 the degree of concave curvature diminished and appeared to be shifting to convex curvature. Figure 7 shows this behavior for Al/Ti = 65.3. This appears to correspond to a loss of first-order deactivation and an increase in the amount of second-order deactivation.

For the Al/Ti molar ratios > 70 the DPF shown in Figure 8 was typical. The curvature now approaches convex that indicates that the deactivation is dominated by second-order processes. A 4-h polymerization run was performed at high Al/Ti and

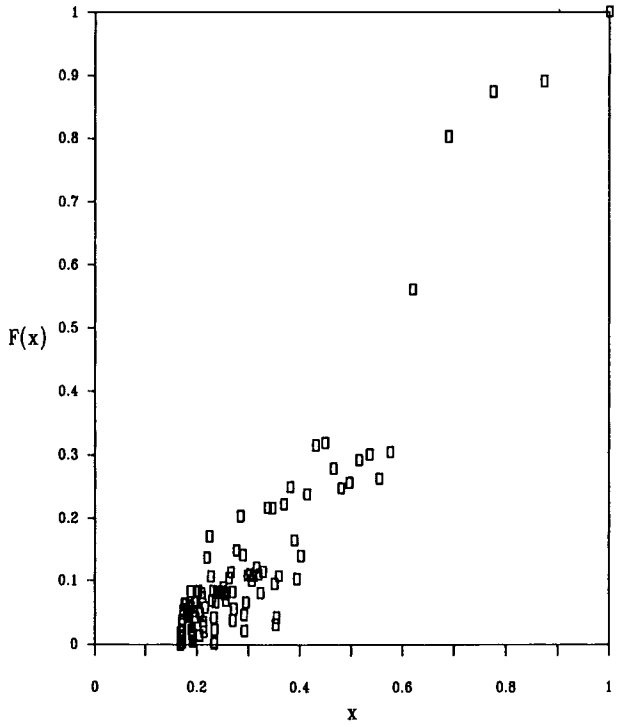

Figure 7 Deactivation profile function (DPF) plot for Al/Ti = 65.3. Polymerization conditions: 40°C, 110 kPa.

first-order deactivation kinetics were exhibited when the time was greater than 3 h. This result seems to indicate that there are relatively stable sites that undergo slow first-order deactivation at both high and low Al/Ti. A second consequence of the DPF plot is that eq. (4) is now the most appropriate form to model the rate kinetics.

The transition of deactivation order from first to second has been observed by Chien and Kuo[18] and Dumas and Hsu[5] for propylene polymerizations. Dumas and Hsu described a sharp transition at Al/Ti = 15 and not the gradual change seen here for ethylene. Chien and Bres[19] found that, for ethylene, second-order deactivation described the kinetics when Al/Ti > 84. For values less than 84 they were noncommittal.

The effect of Al/Ti on the initial activity parameter ($\hat{\theta}_1 = \sum k_{pi} N^*_{i0}$), is shown in Figure 9. Initially $\hat{\theta}_1$ increases until it levels off to a nearly constant value. It appears that as more TEA is used, sites are created until all the potential sites are activated (hence the leveling off). The analysis of the DPF plots (Figs. 6–8) seems to favor this argument because sequential site creation could explain how the deactivation order would change from predominantly first-order to second-order with Al/Ti. It is also possible that all potential sites are activated at

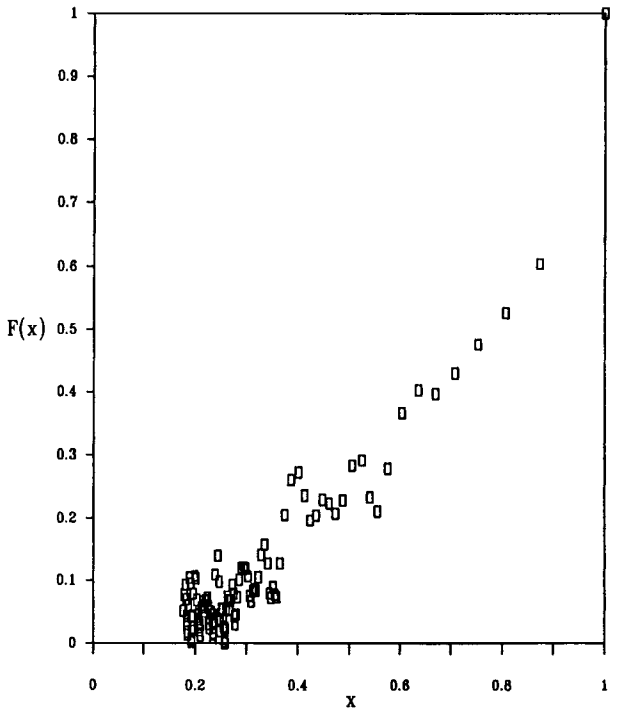

Figure 8 Deactivation profile function (DPF) plot for Al/Ti = 82. Polymerization conditions: 40°C, 110 kPa.

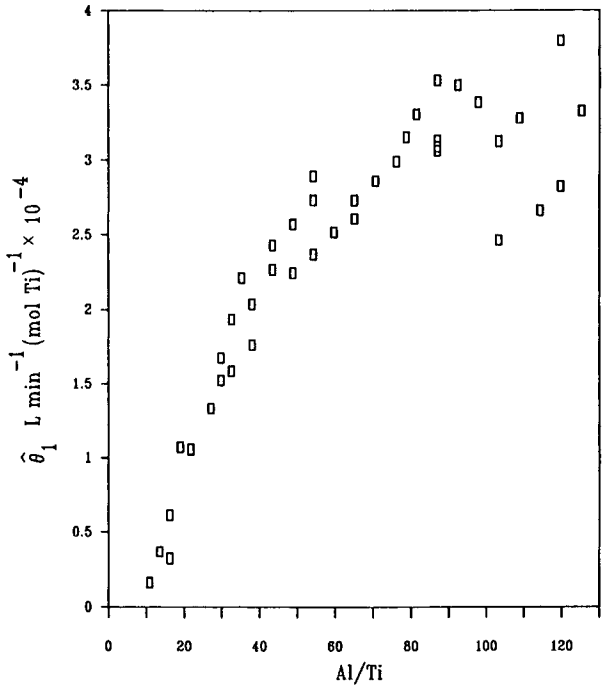

Figure 9 $\hat{\theta}_1$ [L · min^{-1} (mol Ti)$^{-1}$] as a function of Al/Ti. Polymerization conditions: 40°C, 110 kPa.

lower levels of Al/Ti, but further reactions with TEA at higher levels (such as reduction or reductive metathesis) transform sites to a more active state. As all sites are transformed, $\hat{\theta}_1$ levels off. Presumably for such a process to occur active-sites with Ti^{2+} atoms should have comparable or larger propagation rates. However, the literature[16,20] seems to suggest that this is not so. Over-reduced catalysts, with a preponderance of Ti^{2+}, had much lower activities.

It appears that at lower Al/Ti there is a substantial amount of isolated active Ti atoms. The recently proposed structural models of Busico et al.[21] and Chien et al.[14] suggest an isolated active site being an isolated $TiCl_4$ or dimerized (or paired) $TiCl_4$ with only one member of the pair active. Additional site creation by more TEA would involve activation of both the Ti atoms in the pairs, which will lead to second-order deactivation.

The effect of TEA on the deactivation parameter, $\hat{\theta}_2$, is shown in Figure 10. The meaning of $\hat{\theta}_2$ is dependent on the deactivation order. When Al/Ti < 70, $\hat{\theta}_2$ corresponds to the weighted average of k_{di} (the weighting being k_{pi}, the site activity). When Al/Ti > 70, $\hat{\theta}_2$ corresponds to the weighted average of $k_{d2i}C_{i0}^*$ or rather the weighted average of the reciprocal of the deactivation half-life. Initially $\hat{\theta}_2$ increases to a maximum and then decreases. Dumas and Hsu[5] also found that $\hat{\theta}_2$ increased for propylene polymerization with the same catalyst, but observed no maximum. It would appear that isolated sites that are initially produced have larger k_ds. Perhaps isolated Ti moieties in dimers are less stable because of their proximity to unactivated Ti and/or its ligands and vacancies. More TEA seems to create more stable centers through reduction, association, or alkylation processes. Activation of an adjacent Ti in a dimer or pair may also be considered a stabilizing process if an adjacent polymer chain chemically and/or sterically blocks the deactivation mechanism of the polymerizing half of a dimer or pair. This is reflected in the decrease of $\hat{\theta}_2$. It appears that active sites become more stable at higher levels of Al/Ti. This could be caused by more Ti^{2+} being formed, which has a lower activity and probably has a slower deactivation rate. TEA may also associate at the active center, which may result in a more stable site. Slower deactivation at high Al/Ti explains why the productivity continues to increase, even though $\hat{\theta}_1$, the initial activity, levels off.

The DPF analysis found that when Al/Ti was less than 70, first-order deactivation predominates. When there is first-order deactivation, information about the variance ($\hat{\sigma}_w^2$) can be obtained from the least squares parameter estimates. However, the

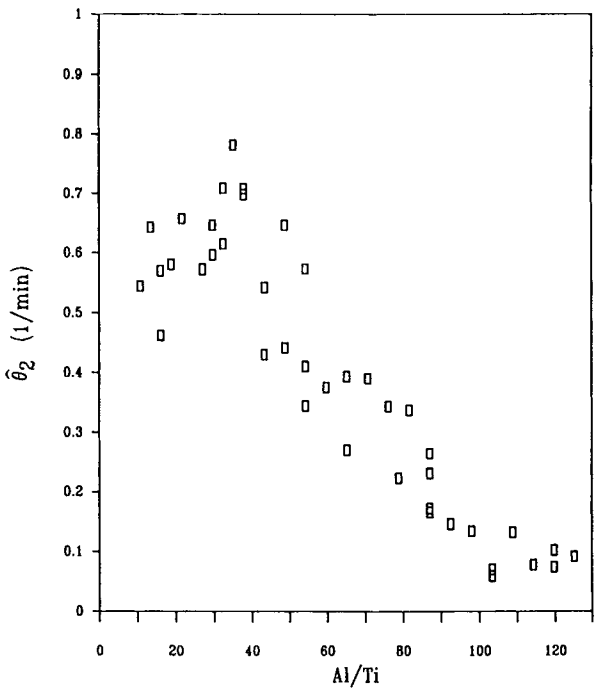

Figure 10 $\hat{\theta}_2$ (min^{-1}) as a function of Al/Ti. Polymerization conditions: 40°C, 110 kPa.

DPF plots (Figs. 6 and 7) resemble simulated DPFs where there is a substantial amount of slow deactivation.[6] When this situation occurred the values obtained for $\hat{\sigma}_w^2$ were not precise.[6] The same difficulty likely occurs here. In addition polymerization rates were lower when Al/Ti < 70 and consequently were more susceptible to experimental errors, which resulted in considerable scatter of the $\hat{\sigma}_w^2$ values. For these reasons $\hat{\sigma}_w^2$ is not expected to give precise results and unfortunately cannot be discussed with any reliability.

When Al/Ti was greater than 70, second-order deactivation predominated and eq. (4) was used. The effect of TEA on the $\hat{\theta}_3$ parameter is shown in Figure 11. Previously it was discussed that $\hat{\theta}_3$ represented a combination of the k_p distribution and site interactions (i.e., deactivation). It is very difficult to decompose $\hat{\theta}_3$ into its constituent parts without precise knowledge of the propagation and deactivation rate constants for each site. Interpretation is therefore restricted to inference from the simulation results.[6] Near Al/Ti = 75, $\hat{\theta}_3$ is around 2.2 and as Al/Ti increases, $\hat{\theta}_3$ decreases to around 1.0. Simulation work suggests that this corresponds to a homogenizing of the second-order deactivation processes. This could be explained if additional TEA produces a more uniform distribution of oxidation states or active site structures. The assumption here is that more

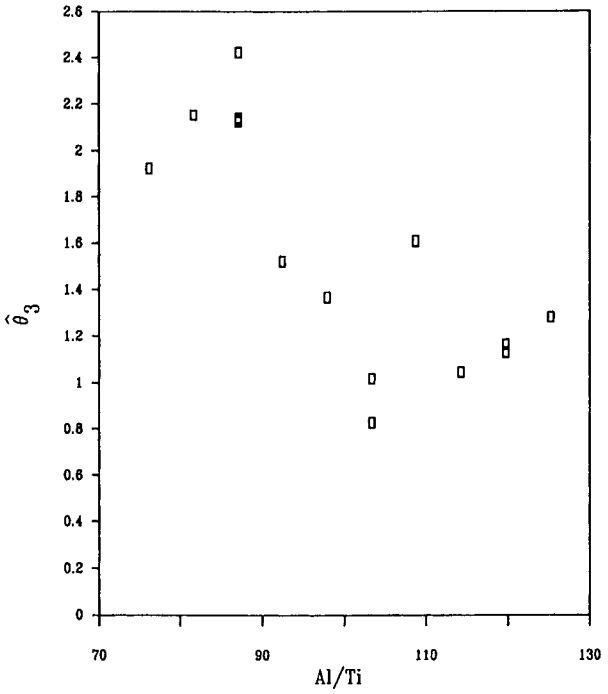

Figure 11 $\hat{\theta}_3$ as a function of Al/Ti. Polymerization conditions: 40°C, 110 kPa.

TEA will produce more Ti^{2+} at the expense of Ti^{3+}.[22] If more Ti^{2+} is present at high Al/Ti then it would appear from $\hat{\theta}_2$ values that a lower oxidation state may result in a more stable site.

Molecular Weight

Modeling the polymerization kinetics with the multisite model provided information about the deactivation processes and initial rate of the catalyst. Information about propagation and transfer reactions is best obtained from the molecular weight analyses of the resulting polymer products. Preliminary analysis of the products using melt index revealed that the polyethylene produced in this system had an extremely high molecular weight (MW). Subsequent GPC (or SEC) analysis confirmed this. The polymers had a $\bar{M}_w \sim 10^6$ and polydispersities (Q) > 10 calculated from the MWD where the high MW portions ($> 2 \times 10^6$) were not completely resolved. Therefore the true $\bar{M}_w$ of the products is likely $> 10^6$ with Q probably larger as well. The polyethylene produced can likely be classified as ultra-high molecular weight polyethylene (UHMWPE).

The high MW is likely a consequence of minimal transfer reactions, with respect to propagation. The transfer reactions of interest are with monomer and the aluminum alkyl. The monomer concentration was quite low (0.0342 mol/L) so it was not surprising that transfer to monomer is not important. Transfer to TEA is usually the most important in slurry polymerizations, but here it clearly is not occurring at a significant rate. The diminished ability of TEA to participate in transfer reactions in a gas-phase system, as compared to a liquid phase reaction, may explain this result. It would seem that the main chain terminating event was site deactivation.

If TEA does not participate in transfer reactions in a significant way then it likely cannot actively participate in other processes, like competitive adsorption with monomer, during the course of polymerization. Consequently models based on competitive adsorption do not appear appropriate here.

To obtain better MWD estimates several experiments were carried out with 5% H_2 in the reaction mixture (the partial pressure of ethylene was still 110 kPa). It has been observed that H_2 can have significant effects on the kinetics in addition to acting as a transfer agent.[23,24] Thus H_2 is not likely to be an "inert" transfer agent. It probably influences the active site distribution and therefore the overall polymerization reactions. The intrinsic catalyst behavior should be similar however.

Figure 12 shows the MWDs, and Table I gives $\bar{M}_w$, $\bar{M}_n$, and Q for various Al/Ti ratios. The molecular weight is still large (500,000–700,000) and the high end tail still appears to be truncated. The polydispersities and $\bar{M}_w$ are very high but show no trend with respect to Al/Ti. Inspection of the MWD curves indicates that at low Al/Ti (26.5) there is a high MW peak and a lower MW shoulder ($\sim$ 100,000). At higher Al/Ti the shoulder becomes part of a broad peak. This could correspond to site creation with lower MW sites being formed preferentially as Al/Ti increases. The lower activity sites could be Ti^{2+} sites formed by further reduction of Ti^{3+}. Beyond Al/Ti = 79 the MWD does not appear to vary too much, seemingly indicating that the propagation characteristics of the catalyst are relatively insensitive beyond this value. Al/Ti > 79 corresponded to the region where activity ($\hat{\theta}_1$) levels off and deactivation becomes predominantly second-order. It would appear that after all the potential sites are formed the propagation characteristics are not changed dramatically.

Mass Transfer Limitation

When the Al/Ti ratio was greater than 130 the polymerization rate curve changes from the decay type of Figure 2, to the acceleration type during the first

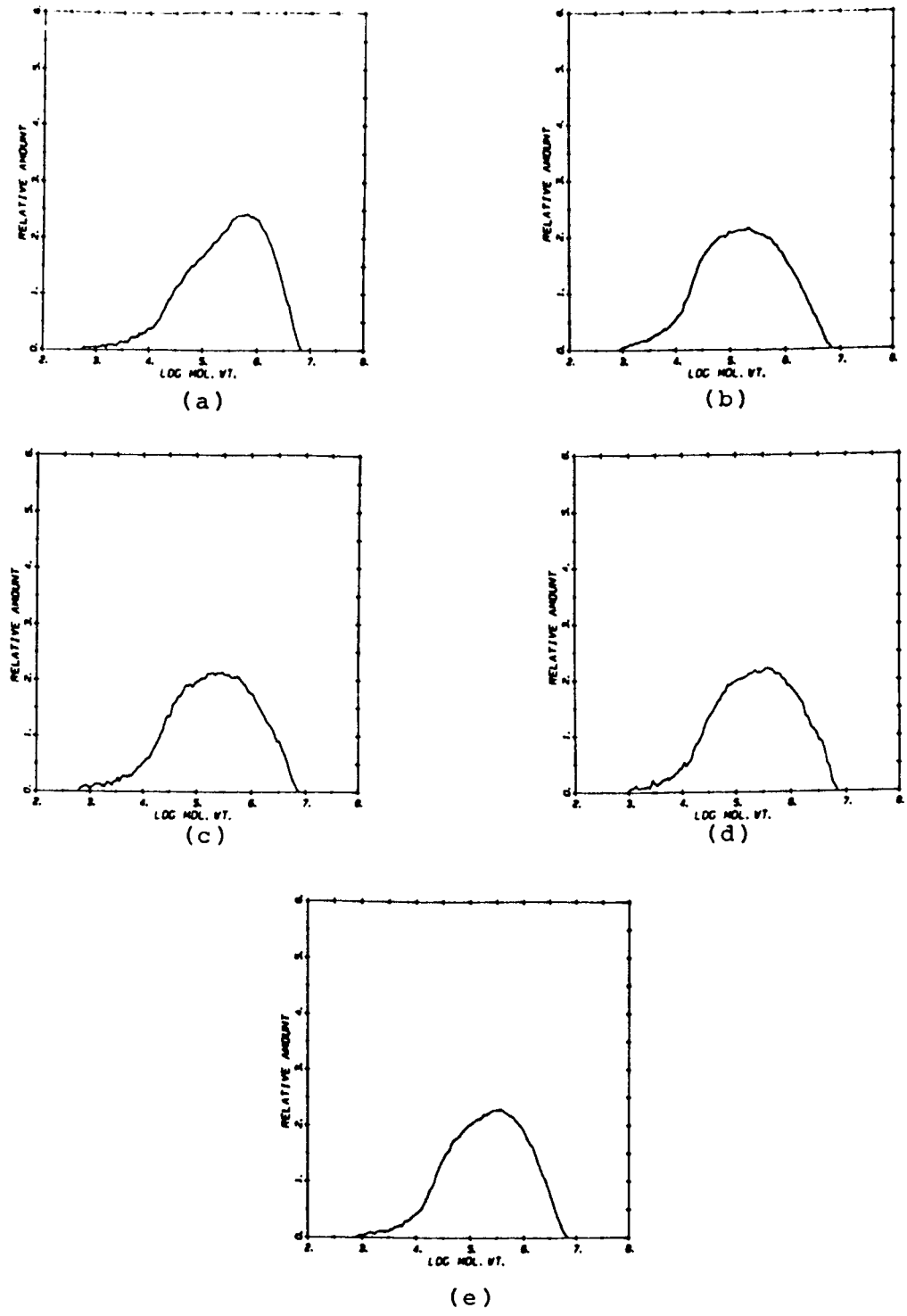

Figure 12 Molecular weight distributions for: (a) Al/Ti = 26.5; (b) Al/Ti = 53; (c) Al/Ti = 79.5; (d) Al/Ti = 100.7; (e) Al/Ti = 119.2. Polymerization conditions: 40°C, 110 kPa.

5 min as shown in Figure 13. Floyd et al.[11] pointed out that when this situation occurred mass transfer resistance was evident.

There are three possible mass transfer limitations discussed in the literature: microparticle diffusion resistance; macroparticle diffusion resistance; and

Table I Molecular Weight Data for Various Al/Ti Ratios

Al/Ti	$\bar{M}_n$	$\bar{M}_w$	Q
26.5	3.80×10^4	6.91×10^5	18.2
53.0	3.08×10^4	4.84×10^5	15.7
79.5	2.75×10^4	5.74×10^5	20.9
100.7	3.87×10^4	6.08×10^5	15.7
119.2	3.82×10^4	5.44×10^5	14.3

monomer sorption rate limitations.[11] The first two were derived from the multigrain physical model of the polymerizing catalyst, where diffusion was thought to occur on two levels: a microparticle level, which was a smaller particle "fractured" off the original macroparticle or initial catalyst particle; and the macroparticle or catalyst particle level. Floyd et al.[11] gave dimensional estimates of the microparticle diameter as ~ 0.006 μm and the macroparticle diameter as that of the initial catalyst particle. Dumas and Hsu[4] examined the catalyst used in this work and found the average catalyst particle diameter was 2 μm. Using this value the extent of diffusion limitation on each particle level can be estimated using the Thiele modulus, ϕ_T, shown in eq. (10).

$$\phi_T = r_c(k_pC^*/\mathcal{D})^{1/2} \tag{10}$$

where r_c is the radius of the (micro- or macro-) particle (cm), $\mathcal{D}$ is the diffusivity (cm^2/s) and k_pC^* is the activity of the catalyst particle and is equivalent to $\hat{\theta}_1 \times (\text{mol Ti})/V_T$ for a total initial polymerizing volume V_T (estimated to be 1.74×10^{-5}L). If $\phi_T > 1$ then diffusion limitations are suspected.

On the microparticle level with $r_c = 0.003$ μm, $\mathcal{D}$ was estimated by Floyd et al.[11] as 10^{-8} $cm^2 \cdot s^{-1}$, which for $\hat{\theta}_1 = 30{,}000$ L/min/(mol Ti) yields $\phi_T = 0.066$. On the macroparticle level $r_c = 1$ μm and $\mathcal{D}$ is estimated at 10^{-4} $cm^2 \cdot s^{-1}$, yielding $\phi_T = 0.22$. From these calculations it appeared that neither of these diffusion processes were significant.

That leaves the monomer sorption rate as the possible limiting factor. If the activity increases to a level in which the rate of monomer consumption by polymerization exceeds the rate at which monomer can be absorbed into the amorphous polymer phase (surrounding the active sites) then the monomer concentration in the amorphous phase will deviate from its equilibrium value with the bulk gas-phase. A requisite assumption here is that polymer near the active site is amorphous, that is, has yet to crystallize until the chain grows away from the site.[8]

This situation is analogous to that which occurs in slurry reactors, where monomer absorption rate is less than polymerization rate, as identified by Dumas and Hsu.[4] However, the surface area available for sorption in this case increases as the polymer particles grow. So it may be possible for the particle to return to kinetic control during the polymerization.

The acceleration type of rate curve during the first 5–8 minutes persisted at all Al/Ti ratios tested above 130. Either the activity, k_pC^*, continued to increase, or deactivation rates continued to decrease.

Effects of Reaction Temperature

The different types of deactivation kinetics at high and low Al/Ti ratios (i.e., above and below 70) resulted in two sets of experiments conducted: at Al/Ti = 98.0, high Al/Ti; and at Al/Ti = 53.0, low Al/Ti.

For ethylene and propylene polymerizations there is typically an optimal temperature for catalyst productivity. For propylene polymerization, using the same catalyst, an optimal temperature of 50°C was observed by Dumas and Hsu.[4] Figure 14 shows the observed ethylene productivity for this catalyst. The optimal temperature is near 40°C when the Al/Ti is high. For a low Al/Ti there is a nearly linear increase with temperature and no optimum. However,

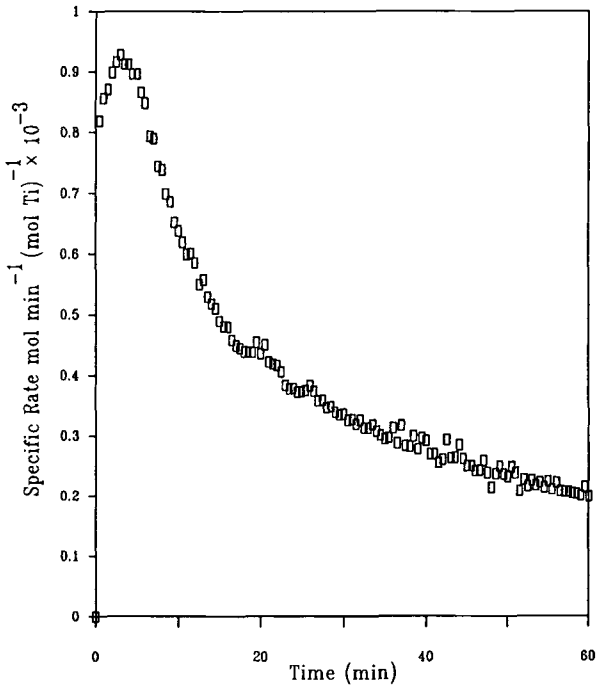

Figure 13 Specific rate [mol·min^{-1} (mol Ti)$^{-1}$] for Al/Ti = 130.6. Polymerization conditions: 40°C, 110 kPa.

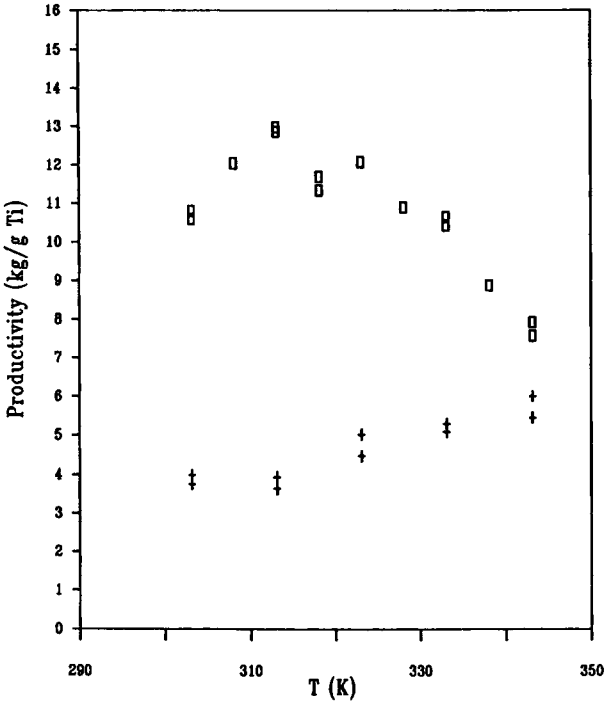

Figure 14 Productivity based on yield ($kg \cdot g^{-1}$ Ti) as a function of temperature. (□) Al/Ti = 98.0; (+) Al/Ti = 50.3 at 110 kPa.

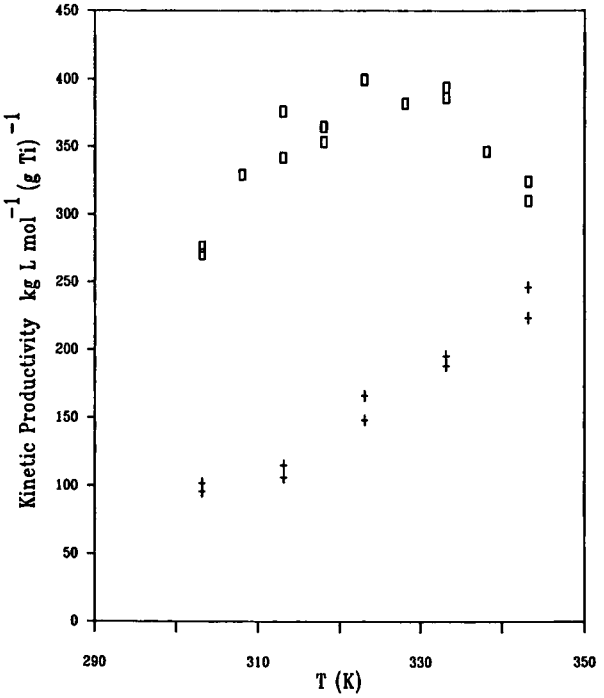

Figure 15 Kinetic productivity [$kg \cdot [M]^{-1}$ (g Ti)$^{-1}$] as a function of temperature. (□) Al/Ti = 98.0; (+) Al/Ti = 50.3 at 110 kPa.

this analysis fails to account for the temperature dependence of concentration of sorbed monomer in the amorphous phase. Equation 2 describes the relationship between Henry's Law constant, k^*, and temperature, which in turn determines the monomer concentration. If the yields of these experiments are normalized so that this dependence is removed (by dividing by $[M]$), a "kinetic productivity" can be calculated. These values are shown in Figure 15. The optimal temperature for high Al/Ti is now approximately 55°C and the same nearly linear trend for low Al/Ti is observed.

The origin of the optimum at high Al/Ti can be found by examining Arrhenius plots (Figs. 16, 17) of the multisite model parameters. At higher temperatures $\hat{\theta}_1$ (shown in Fig. 16), the initial activity parameter, decreases, but $\hat{\theta}_2$ (as shown in Fig. 17), the deactivation parameter, increases.

Curvature of Arrhenius plots can provide evidence that there are multiple active sites. Curvature should be expected here, however, the parameters $\hat{\theta}_1$ and $\hat{\theta}_2$ are lumped with concentration of active sites making such an interpretation more difficult. In addition, the temperature range was not very broad, meaning that the full extent of activation energy differences may not be seen. For $\hat{\theta}_1$ at high Al/Ti

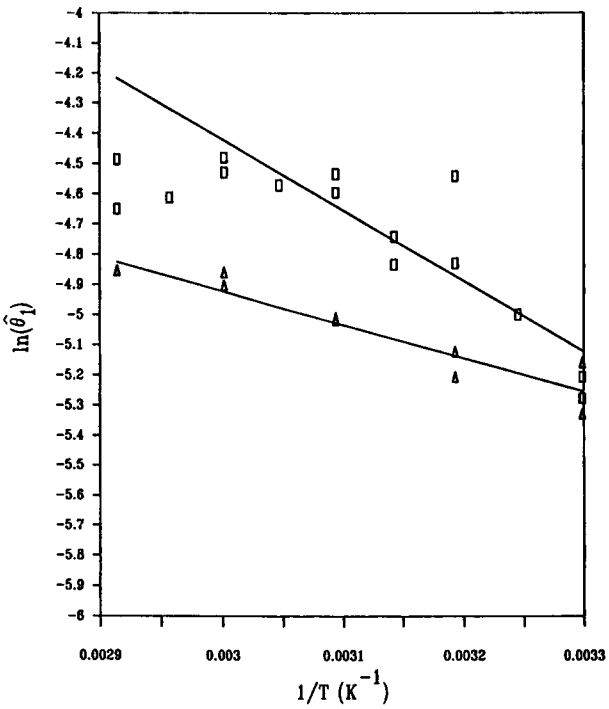

Figure 16 Arrhenius plot for $\hat{\theta}_1$. (□) Al/Ti = 98.0; (△) Al/Ti = 50.3 at 110 kPa.

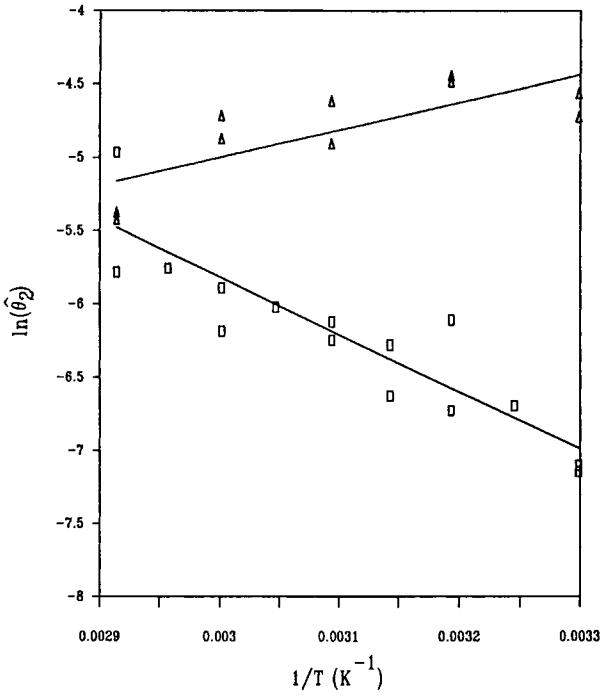

Figure 17 Arrhenius plot for $\hat{\theta}_2$. (□) Al/Ti = 98.0; (△) Al/Ti = 50.3 at 110 kPa.

curvature is definitely present with $\ln(\hat{\theta}_1)$ increasing until 60°C then dropping off. This could be because of loss of C^* from site destruction at higher temperature, as has been suggested by Guastalla and Giannini,[25] Barbé et al.,[26] and Keii et al.[17] Between 30 and 60°C the apparent activation energy (E_a) was estimated as 19.5 ± 3.3 kJ/mol.

At low Al/Ti, $\ln(\hat{\theta}_1)$ is nearly linear, although there may be some drop off at 70°C. The apparent E_a for this case is 9.3 ± 1.1 kJ/mol. Chien and Bres[19] found that apparent activation energies for ethylene propagation ranged from 25.5 to 41.0 kJ/mol for a $MgCl_2$/EB/*p*-cresol supported catalyst. For a $MgCl_2/SiO_2/TiCl_4$ catalyst Kim et al.[27] and Spitz et al.[3] found apparent E_a values (for ethylene) of 49.9 kJ/mol and 56.9 kJ/mol, respectively, the latter from a gas-phase system. A value of 41.8 kJ/mol has been suggested as a reasonable estimate by Floyd et al.[11] Both E_a/s found in this study were less than these values. A similar result was found in the gas-phase propylene polymerization where the E_a was approximately half that for slurry polymerization.[2,17] Tang[28] has speculated that lower apparent E_a values in gas-phase reactors could be the result of "the monomer not having the additional resistance of solvent molecules." Hutchinson and Ray[8] have proposed that the differences in apparent E_a between slurry and gas-phase reactors are caused by normalization of the Arrhenius plots with the incorrect monomer concentration. If the bulk monomer concentration of the slurry reactor was replaced with the sorbed monomer concentration in the amorphous phase, then the apparent E_a values for gas-phase and slurry reactors were in general agreement.

Figure 17 shows the Arrhenius plot for $\hat{\theta}_2$. At high Al/Ti, $\ln(\hat{\theta}_2)$ exhibits nearly linear behavior with an E_a of 35.6 ± 5.0 kJ/mol. However, if decreased C^* explains the drop off in $\hat{\theta}_1$ then k_{d2} must increase, since $\hat{\theta}_2$ is the weighted average of $k_{d2i}C^*_{i0}$. This compensation effect may linearize the Arrhenius plot.

At low Al/Ti $\ln(\hat{\theta}_2)$ decreases with increasing temperature with an apparent E_a of −15.5 ± 4.4 kJ/mol between 30 and 70°C. It should be pointed out that a slope of zero (a horizontal line) falls in the 95% confidence interval, meaning that this parameter may be independent of temperature over this range. These results imply that first-order deactivation is stabilized or independent of temperature and is further indication that the fast first-order deactivation reactions are complex, probably involving more then one reaction step.

Figure 18 shows the behavior of $\hat{\theta}_3$ as a function of temperature. As temperature increases $\hat{\theta}_3$ increases from approximately 1.0 at 30°C to near 2 at 70°C. The interpretation is that higher temperatures create a more heterogeneous distribution of second-

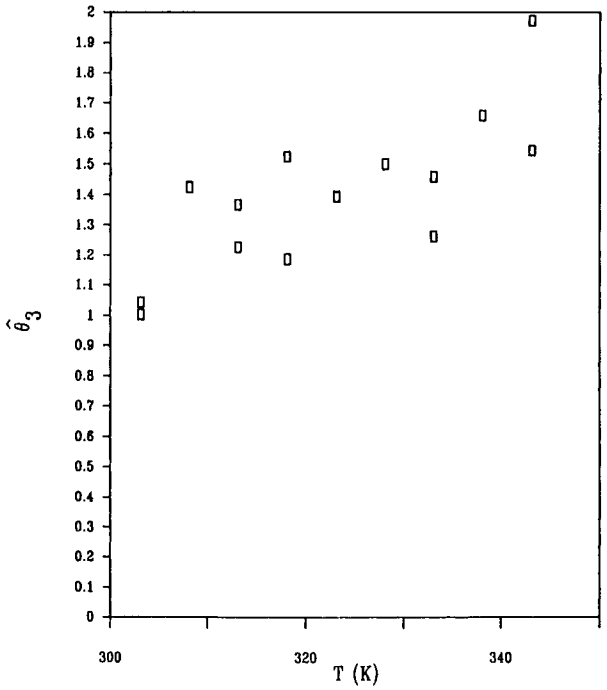

Figure 18 $\hat{\theta}_3$ as a function of temperature. Polymerization conditions: Al/Ti = 98.0, 110 kPa.

order deactivation reactions. Molecular weight distribution data from Jejelowo et al.,[29] where the polydispersities of polyethylenes produced from a $MgCl_2/SiO_2/TiCl_4$ + TEA catalyst increased with temperature, seem to confirm this result.

CONCLUSIONS

A gas-phase polymerization reactor was developed to study the polymerization rate kinetics of the $MgCl_2/EB/TiCl_4$ + TEA Ziegler–Natta catalyst. Together with a novel catalyst injection system, reproducible rate data were produced. The multisite model was used to examine the polymerization rate kinetics of ethylene. The Al/Ti molar ratio was studied and it was demonstrated that the amount of TEA used had significant effects on the kinetics.

1. As Al/Ti increased from zero, deactivation order changed from predominantly first- to second-order. The order transition occurred progressively with Al/Ti = 70 being the crossover point between the two types of kinetics.
2. At low Al/Ti (< 70) at least two types of first-order deactivation processes seem to occur, one fast and one slow.
3. At high Al/Ti (> 70) deactivation was predominantly second-order, with what seems to be underlying slow first-order deactivation.
4. Catalyst productivity increased with Al/Ti monotonically within the range (10–125) studied.
5. Multisite modeling results indicated that initial activity increased with Al/Ti, then leveled off when Al/Ti > 70 and approached to what appeared to be a maximum potential activity. As Al/Ti increased, the deactivation rate increased to a maximum, then decreased as the kinetics became predominantly second-order. At higher Al/Ti the dispersion of deactivation reactions was reduced. These results appeared consistent with progressive site activation where, at low Al/Ti, sites were mostly isolated and as Al/Ti increased more sites became adjacent resulting in second-order deactivation.
6. The molecular weight of the polyethylene produced was very high ($> 10^6$). Analysis of MWDs of polymers produced with 5% H_2 showed that $\bar{M}_w$ and MWD were relatively insensitive to Al/Ti when it was greater than 70. Below that a lower MW shoulder was detected. The shoulder became part of a broader peak at high Al/Ti ratio.
7. When Al/Ti ratio was greater than 130 the polymerization rate curve changed from straight decay to initial acceleration followed by the normal decay behavior, indicating clearly a monomer–sorption rate limitation.

The temperature effects, over a range of 30–70°C, on polymerization were dependent on the Al/Ti ratio:

1. At high Al/Ti there was an optimum in catalyst productivity at 55°C. The apparent activation energy for initial activity (i.e., $\hat{\theta}_1$, the initial activity or $\sum k_{pi} N^*_{i0}$) was found to be 19.5 ± 3.3 kJ/mol. A drop-off of the Arrhenius plot at higher temperatures (70°) may be due to C^* destruction. The observed activation energy for deactivation ($\hat{\theta}_2$) was found to be 35.6 ± 5.0 kJ/mol. $\hat{\theta}_3$, a qualitative measure of dispersity, increased from approximately 1 to 2 with temperature, and indicated a greater dispersity of second-order deactivation reactions with temperature.
2. At low Al/Ti the productivity increased linearly with temperature. The apparent activation energy for initial activity was found to be 9.3 ± 1.1 kJ/mol. The apparent E_a for deactivation ($\hat{\theta}_2$) was found to be −15.5 ± 4.4 kJ/mol, although an apparent E_a of zero falls in the 95% confidence interval indicating that deactivation at low Al/Ti may be independent of temperature.

The authors wish to thank the Natural Sciences and Engineering Research Council of Canada for financial support for this work, and to Ron Murray of the Du Pont Research Centre of Canada for performing the molecular weight analyses.

NOMENCLATURE

Al/Ti	Molar ratio of aluminum alkyl to titanium in the catalyst that was used
C^*	Total concentration of active sites
C_i^*	Concentration of active species i
$\mathcal{D}$	Diffusivity of monomer, $cm^2 \cdot s^{-1}$
DPF	Deactivation profile function
$E(\ )$	Expected value (mean)
E_a	Apparent activation energy, $kJ \cdot mol^{-1}$
EB	Ethylbenzoate
$F(x)$	Deactivation profile function

k^*	Henry Law constant, $mol \cdot V_{ap} \cdot atm^{-1}$
k_{di}	First-order deactivation rate constant for species i, s^{-1}
k	Second-order deactivation rate constant for species i, $L \cdot mol \cdot s^{-1}$
k_{pi}	Propagation rate constant for species i, $L \cdot mol \cdot s^{-1}$
MW	Molecular weight
$\bar{M}_w$	Weight average molecular weight
$\bar{M}_n$	Number average molecular weight
$[M]$	Monomer concentration at the active sites, $mol \cdot V_{ap}^{-1}$
$[M]_b$	Bulk monomer concentration, $mol \cdot L^{-1}$
N	Number of active sites species
N_i^*	Number of moles of active sites
P	Pressure, atm or kPa
Q	Polydispersity ($\bar{M}_w/\bar{M}_n$)
Rp	Rateofpolymerization,$mol \cdot L^{-1} \cdot min^{-1}$
Rp_i	Rate of polymerization for species i, $mol \cdot L^{-1} \cdot min^{-1}$
Re	Reynolds number
r_c	Radius of catalyst particle, cm
t	Time, min
T_c	Critical temperature for monomer, K
TEA	Triethylaluminum
UV-VIS	Ultraviolet-visible
UHMWPE	Ultra high molecular weight polyethylene
V_{ap}	Volume of amorphous polymer, L
V_T	Total volume in which polymerization occurs, L
x	Fractional activity (Rp/Rp_0) with respect to initial activity

Greek Symbols

α	Shape parameter of gamma distribution
β	Parameter of rate equation based on binominal DPF
ϕ_T	Thiele modulus
η	Parameter describing the relationship between active site components and the index i
μ	Weighted (by activity) mean of deactivation rate constant distribution
ν	Parameter of rate equation based on binomial DPF
θ_1	Initial activity parameter
θ_2	Initial deactivation rate parameter
θ_3	Dispersion parameter for deactivation parameter
σ^2	Weighted (by activity) variance of deactivation rate constant distribution

Subscripts

i	Indicates ith species of sites or index of components with $i = 1, 2, 3, \ldots,$
0	Indicates initial conditions at $t = 0$

Overscript

Indicates a least squares estimate

REFERENCES

1. D. T. Lynch and S. E. Wanke, *Can. J. Chem. Eng.*, **69,** 332 (1991).
2. Y. Doi, M. Murata, K. Yano, and T. Keii, *Ind. Eng. Chem. Prod. Res. Dev.*, **21,** 580 (1982).
3. R. Spitz, V. Pasquet, and A. Guyot, *Transition Metals and Organometallics as Catalysts for Olefin Polymerizations,* W. Kaminsky and H. Sinn, Eds., Springer-Verlag, New York, 1988, p. 405.
4. C. Dumas and C. C. Hsu, *J. Appl. Polym. Sci.*, **37,** 1605 (1989).
5. C. Dumas and C. C. Hsu, *J. Appl. Polym. Sci.*, **37,** 1644 (1989).
6. J. J. A. Dusseault, Ph.D. Thesis, Queen's University, Kingston, Canada, 1991.
7. A. I. Vogel, *Quantitative Inorganic Analysis: Theory and Practice,* 2nd ed., Longmans, Green and Co., London, 1951.
8. R. Hutchinson and W. H. Ray, *J. Appl. Polym. Sci.*, **41,** 51 (1990).
9. S. A. Stern, J. T. Mullhaupt, and P. J. Gareis, *AIChE. J.*, **15,** 64 (1969).
10. S. Floyd, K. Y. Choi, T. W. Taylor, and W. H. Ray, *J. Appl. Polym. Sci.*, **31,** 2231 (1986).
11. S. Floyd, K. Y. Choi, T. W. Taylor, and W. H. Ray, *J. Appl. Polym. Sci.*, **32,** 2935 (1986).
12. J. J. A. Dusseault, M. F. Cunningham, C. Dumas, and C. C. Hsu, *Transition Metal Catalyzed Polymerizations: Ziegler-Natta and Metathesis Polymerizations,* R. P. Quirk, Ed., Cambridge University Press, Cambridge, UK, 1988, p. 136.
13. M. F. Cunningham, M.Sc. Thesis, Queen's University, Kingston, Ontario, Canada, 1987.
14. J. C. W. Chien, S. Weber, and Y. Hu, *J. Polym. Sci., A, Polym. Chem.*, **24,** 1499 (1989).
15. C. Dumas and C. C. Hsu, *Chem. Eng. Commun.*, **24,** 37 (1983).
16. K. Soga, S. Chen, and R. Ohnishi, *Polym. Bull.*, **8,** 261 (1982).
17. T. Keii, E. Suzuki, M. Tamura, M. Murata, and Y. Doi, *Makromol. Chem.*, **183** (1982).
18. J. C. W. Chien and J. Kuo, *J. Polym. Sci.: Polym. Chem. Ed.*, **23,** 731 (1985).
19. J. C. W. Chien and P. Bres, *J. Polym. Sci., A, Polym. Chem.*, **24,** 1967 (1986).

20. N. Kashiwa and X. Yoshitake, *J. Makromol. Chem.*, **185,** 1133 (1984).
21. V. Busico, P. Corradini, L. De Martino, A. Proto, and E. Albizzati, *Makromol. Chem.*, **187,** 1115 (1986).
22. J. Boor, Jr, *Ziegler-Natta Catalysts and Polymerizations,* Academic Press Inc., New York, 1979.
23. T. Keii, *Transition Metal Catalyzed Polymerizations: Ziegler-Natta and Metathesis Polymerizations,* R. P. Quirk, Ed., Cambridge University Press, Cambridge, UK, 1988.
24. J. C. W. Chien and T. Nozaki, *J. Polym. Sci., A: Polym. Chem.*, **39,** 505 (1991).
25. G. Guastalla and U. Giannini, *Makromol. Chem., Rapid Commun.*, **4,** 519 (1983).
26. P. C. Barbé, G. Cecchin, and L. Noristi, *Adv. Polym. Sci.*, **81,** 1 (1987).
27. I. Kim, J. H. Kim, and S. I. Woo, *J. Appl. Polym. Sci.*, **39,** 837 (1990).
28. S. Tang, *Studies Surf. Sci. Catalysis,* **25,** 165 (1986).
29. M. O. Jejelowo, D. T. Lynch, and S. E. Wanke, *Macromolecules,* **24,** 1755 (1991).

Received March 5, 1992
Accepted February 23, 1993